Simulations of non-uniform embossing: the effect of asymmetric neighbor cavities on polymer flow during nanoimprint lithography

H. D. Rowland, W. P. King, A. C. Sun, and P. R. Schunk

Sandia National Laboratories

Simulations of non-uniform embossing: the effect of asymmetric neighbor cavities on polymer flow during nanoimprint lithography

Harry D. Rowland[1], William P. King[1], Amy C. Sun[2], P. Randy Schunk[3]

[1]Woodruff School of Mechanical Engineering
Georgia Institute of Technology
Atlanta, GA 30329-0405

[2] Geohydrology
[3] Multiphase Transport Processes
Sandia National Laboratories
P.O. Box 5800
Albuquerque, New Mexico 87185-1351

Abstract

This paper presents continuum simulations of viscous polymer flow during nanoimprint lithography (NIL) for embossing tools having irregular spacings and sizes. Simulations varied non-uniform embossing tool geometry to distinguish geometric quantities governing cavity filling order, polymer peak deformation, and global mold filling times. A characteristic NIL velocity predicts cavity filling order. In general, small cavities fill more quickly than large cavities, while cavity spacing modulates polymer deformation mode. Individual cavity size, not total filling volume, dominates replication time, with large differences in individual cavity size resulting in non-uniform, squeeze flow filling. High density features can be modeled as a solid indenter in squeeze flow to accurately predict polymer flow and allow for optimization of wafer-scale replication. The present simulations make it possible to design imprint templates capable of distributing pressure evenly across the mold surface and facilitating symmetric polymer flow over large areas to prevent mold deformation and non-uniform residual layer thickness.

Acknowledgments

Contents

Figures

Nomenclature

NIL	nanoimprint lithography
P	applied load
η	polymer viscosity
t	fill time
S	indenter width
S_i	inner indenter width
S_o	outer indenter width
S_{MAX}	maximum indenter width
W	cavity half width
W_i	inner cavity half width
W_o	outer cavity half width
h_i	initial polymer film thickness
h_c	cavity height
t_o	time to onset of filling
t_f	time when polymer has covered half master cavity floor
h_r	residual film thickness

1. Executive Summary

Nanoimprint lithography (NIL) is a high resolution, high-throughput, economical alternative to standard silicon based fabrication technologies. For NIL to become a viable manufacturing technology, a deep understanding of both local polymer flow within simple geometries and global polymer flow between largely spaced fields is required for rational process and master tool design. This paper presents continuum simulations of viscous polymer flow during nanoimprint lithography (NIL) for embossing tools having irregular spacings and sizes.

Simulations investigate embossing of nonuniform rectilinear cavities of viscous dominant flows with no elastic stress relaxation, i.e. Reynold's number << 1, Deborah number << 1, and Capillary number >> 1. A uniform pressure applied to the silicon cavity presses the indenter into the viscous polymer film. No-slip conditions prescribed at the polymer-indenter and polymer-substrate interface model the contact while a capillary surface with surface tension captures the physics of the free polymer surface. Independent variation of film thickness, cavity width, and indenter width or cavity spacing of side-by-side non-uniform geometries allows examination of parameters most significantly governing global polymer deformation and filling. Filling of single cavities affects neighboring cavities, as differences in individual cavity size dominate global tool replication time, resulting in non-uniform, squeeze flow filling.

For global mold filling, characteristic NIL filling times of individual cavities determines order of local cavity filling. Relative cavity size and indenter width govern local polymer deformation. Large differences in cavity size lead to non-uniform filling and non-local polymer flow. Maximum indenter width governs filling time with a quadratic dependence and the rapid filling of small cavities results in an increase in effective maximum indenter width eventually leading to global squeeze flow. Knowledge of local filling order allows determination of global polymer flow direction and factors limiting global embossing. High density features can be modeled as a solid indenter in squeeze flow to accurately predict polymer flow and allow for optimization of wafer-scale replication. Local filling of small cavities should be accommodated by designing embossing tools with symmetric filling over the total stamp area to reduce tool warping. The present simulations allow global mold design for simultaneous full replication of large-scale and nanoscale patterns and near-uniform residual layer thickness over a predicted time scale.

2. Introduction

Nanoimprint lithography (NIL) is a high resolution [1], large scale [2] thermomechanical manufacturing process where a nanostructured master tool is pressed into a thermoplastic polymer at elevated temperature, forming a negative replica of the master in the polymer substrate. The high throughput process offers an economical alternative to standard silicon based fabrication technologies for nanoelectronics or nanoelectromechanical systems (NEMS). Practical implementation of NIL will require multiple non-uniform-sized feature geometries on a single tool, while retaining small and uniform residual layer thickness. A deep understanding of both local polymer flow in simple geometries and of global polymer flow in irregular fields is required for rational process and master tool design. This paper presents simulations embossing molds of non-uniform feature sizes and spacings into viscous polymer to investigate polymer flow and mold filling time during NIL.

Previous experiments and simulations investigating hot embossing manufacturing (HEM) and NIL have focused on understanding polymer flow in simple uniform geometries or single indenter tools [3-10]. Factors influencing polymer flow have included shear deformation, elastic stress release, non-linear rubber-like elastic dynamics, capillary flow, and viscous flow. In general, deformation mode was found to depend on geometric flow restrictions and time scale of flow [10].

A few groups have studied large-scale flow field effects with non-uniform embossing tools [11-14], noting limitations in simultaneous replication of patterns having large and small features in close proximity. Correlation and crosstalk of stress and flow fields of simple geometries arises when a single embossing tool contains multiple, non-uniform feature geometries. Non-uniform filling increases the tool-polymer contact area, slowing the speed of imprint. Viscous polymer flow over large areas limits full replication and uniformity of residual layer thickness as incomplete filling and tool warping result due to non-uniform deformation. Simultaneous replication of combined features having significantly different sizes requires long imprint times compared to uniform fields [11-13, 15]. Step and Flash NIL, laser-assisted NIL, and one-step imprint-photolithography can displace a smaller volume of material and/or imprint at lower viscosities than conventional embossing [15-17], but conventional embossing is more robust for materials compatibility.

This paper presents simulations of viscous polymer deformation during NIL embossing with non-uniform embossing tools. Independent variation of cavity width and indenter width or cavity spacing of side-by-side non-uniform geometries allows examination of parameters governing polymer deformation and filling time. Characteristic NIL velocity, V_{NIL}, of local cavities governs order of complete cavity filling, indenter width determines order of onset of filling, and individual cavity size difference dominates overall replication time for shear and squeeze flow. Small cavity sizes generally fill first though cavities filling via constrained single peak deformation require long filling times. Non-uniform filling leads to squeeze flow dominated global filling, suggesting that process

design should model high density feature areas as a solid indenter to direct global polymer flow and distribute mold pressure evenly.

3. Simulation Overview

Previous simulations of NIL modeled a single repeating embossing cavity with the polymer as a viscous liquid [8, 10] or nonlinear solid elastic [6, 7]. Recent CFD studies modeling the polymer as a viscous liquid simulated a few variations of multiple cavity embossing with non-uniform spacing [18]. The present work uses the finite element multi-physics code *GOMA* to model the moving boundary polymer surface in NIL. An applied force on a rigid silicon indenter presses the embossing tool into the viscous Newtonian liquid polymer. Details of the simulation parameters and boundary conditions are described elsewhere [10]. Briefly, both the liquid polymer and solid indenter are modeled using an arbitrary Lagrangian/Eulerian reference frame [19, 20]. No-slip conditions are applied at the indenter-polymer and polymer-substrate interface and a surface tension is applied to the free surface of the polymer. Figure 1 shows a representative non-uniform three-cavity geometry with outer non-symmetric cavities and an inner symmetric cavity. Outer indenter width, outer cavity width, inner indenter width, and inner cavity width are systematically varied to determine which geometric factors govern polymer deformation and cavity filling time. Simulations of a simple two-cavity geometry further investigate the effects of varying indenter widths on replication time.
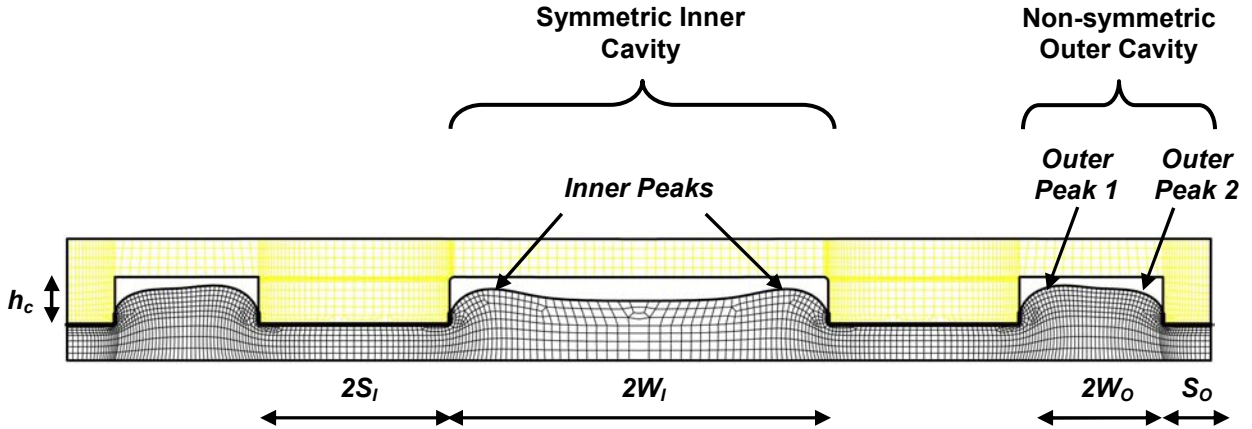

Figure 1. Example non-uniform geometry embossing tool showing symmetric inner and non-symmetric outer cavities.

4. Results

Simulations investigate embossing of non-uniform geometries into viscous dominant flows with no elastic stress relaxation, i.e. Reynold's number << 1, Deborah number << 1, and NIL Capillary number >> 1 [10]. Analysis of the motion of polymer peaks and the differing individual cavity fill times and global fill times allows determination of parameters governing non-uniform embossing.

Cavity filling order depends on local cavity size and filling mode. Figure 2 shows filling modes of non-uniform embossing for both shear and squeeze flows. Local cavity size, defined as the ratio of local cavity width to local tool width, generally predicts which cavities fill first, with smaller cavity sizes filling before larger cavity sizes. Figure 2a,b shows cavity filling of squeeze flow with smaller cavities filling before larger cavities. In cavities having dual peak deformation, the polymer peak nearest the largest indenter width will vertically deform faster than the polymer peak nearest the smallest indenter. In Fig. 2a, more polymer is displaced by the inner indenter than is displaced by the outer indenter, causing the polymer peak nearest the inner cavity to reach the mold first. The indenter width determines which side of a cavity begins filling first, while the cavity size determines which cavity fills first. Figure 2c,d shows cavity filling of shear flow where smaller cavity sizes do not always fill before larger cavity sizes, with small cavity sizes filling first in Fig. 2c and large cavity sizes filling first in Fig. 2d. The size of the single peak cavity strongly influences filling order. When the cavity size is sufficiently small, constrained single peak flow occurs, resulting in large cavity sizes filling before small cavity sizes. Constrained single peak flow occurs when the local cavity half width is less than approximately half the film thickness. The order of filling for individual cavities can be predicted by comparing the appropriate shear flow, squeeze flow, or single peak flow V_{NIL} [10] for all the individual cavities on a mold.
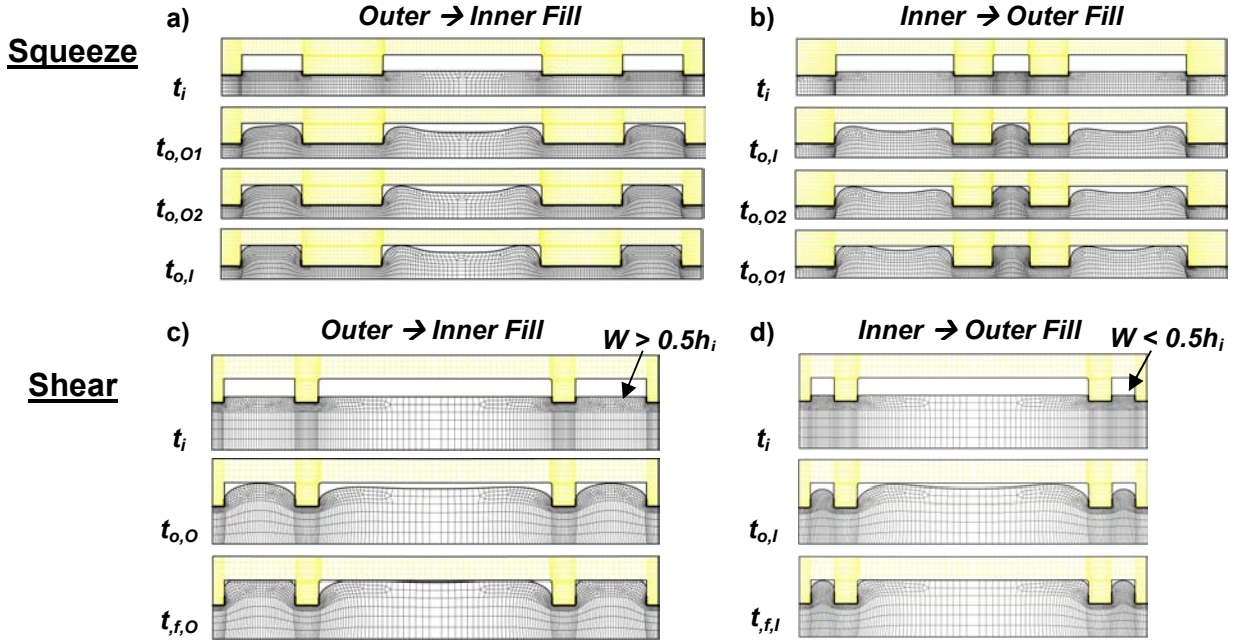
Figure 2. Deformation profiles for possible onset deformation modes of (a,b) squeeze flow and (c,d) shear flow. (a,b) The smallest cavity size fills first in squeeze flow, with the direction of the polymer peak governed by the maximum indenter width. (c,d) In shear flow, the smallest cavity size fills first unless the local cavity half width (W) is less than half the film thickness ($0.5h_i$). When $W < 0.5h_i$, hydrostatic stress in the small cavity slows filling, allowing large cavity sizes to fill first. V_{NIL} can predict cavity filling order.

The difference in adjacent cavity filling times increases as the local cavity size difference increases, forcing more polymer to be displaced over larger distances than in a uniform deformation field. Figure 3 shows the effects of decreasing inner cavity size due to an increasing inner indenter width. As the inner indenter width increases, more polymer is available to fill the cavity, and the excess polymer is forced longer distances to fill the remaining vacant cavities than for the case of a smaller indenter width. Figure 3b shows the polymer peak nearest the inner cavity is pushed away from the sidewall as filling progresses and the polymer peak farthest the inner cavity is pushed towards the sidewall as inner indenter width increases. The increase in inner indenter width increases the amount of displaced polymer, resulting in a dramatic rise in time to fill for the outer cavity and global filling of the embossing tool, as shown in Fig. 3c. The increase in inner indenter width has little effect on the filling time of the inner cavity, since ample polymer is locally available to fill the cavity and single peak flow is limited by the flow of polymer into the cavity, not the flow of the indenter into polymer [10]. As the ratio of polymer available to polymer required for local cavity filling increases, long range flow effects develop causing polymer transport between global tool sections, as noted in [13]. Figure 3c shows total time to fill increasing with increasing inner indenter width and total indenter width, i.e. the sum of the inner and outer indenter width. To determine whether
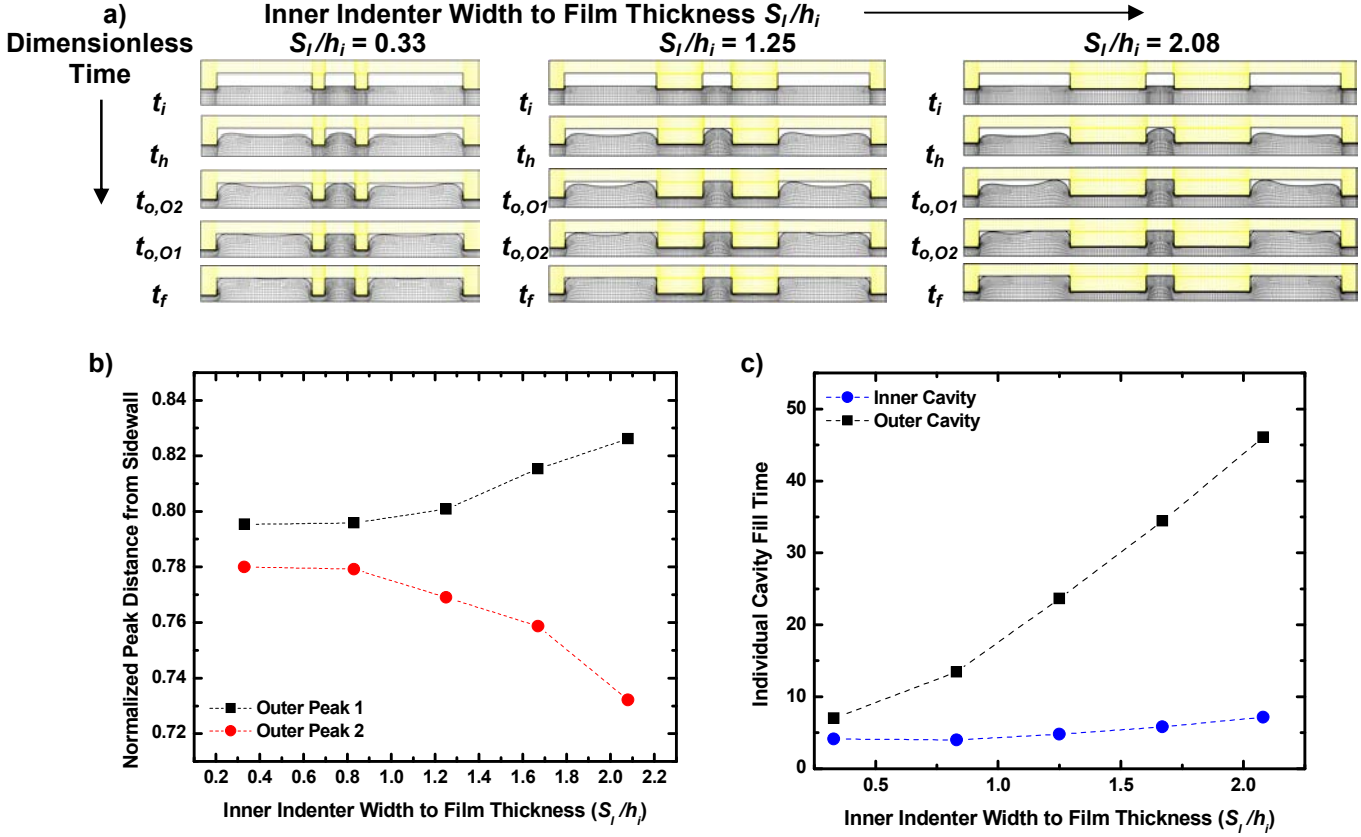
Figure 3. (a) Deformation profiles for increasing inner indenter width. (b) The increased material forced from beneath the inner cavity and indenter pushes the outer peak 1 away from the sidewall and outer peak 2 closer to the sidewall while (c) dramatically increasing the fill time of the outer cavity.

the total indenter width or the maximum single indenter width, i.e. the greater of the inner or outer indenter width, governs fill time, a simple two cavity geometry was modeled. Figure 4 shows the change of fill time due to maximum indenter width in the two cavity geometry. For constant total indenter width and varying maximum indenter width, dramatically different fill times result. The fill times depend not on total indenter width but instead on maximum indenter width. Viscous flow theory of a thin layer of fluid between plates, using the lubrication approximation, predicts a quadratic dependence of fill time on indenter width. The quadratic dependence of fill time on maximum indenter width observed here results in a characteristic NIL fill time approximated by

$$t_{NIL} = \frac{\eta S_{MAX}^{2}}{2P}\left(\frac{1}{h_r^2} - \frac{1}{h_i^2}\right),\qquad(1)$$

where η is the polymer viscosity, S_{MAX} is the maximum indenter width, P is the embossing pressure, h_r is the residual film thickness, and h_i is the initial film thickness [10].
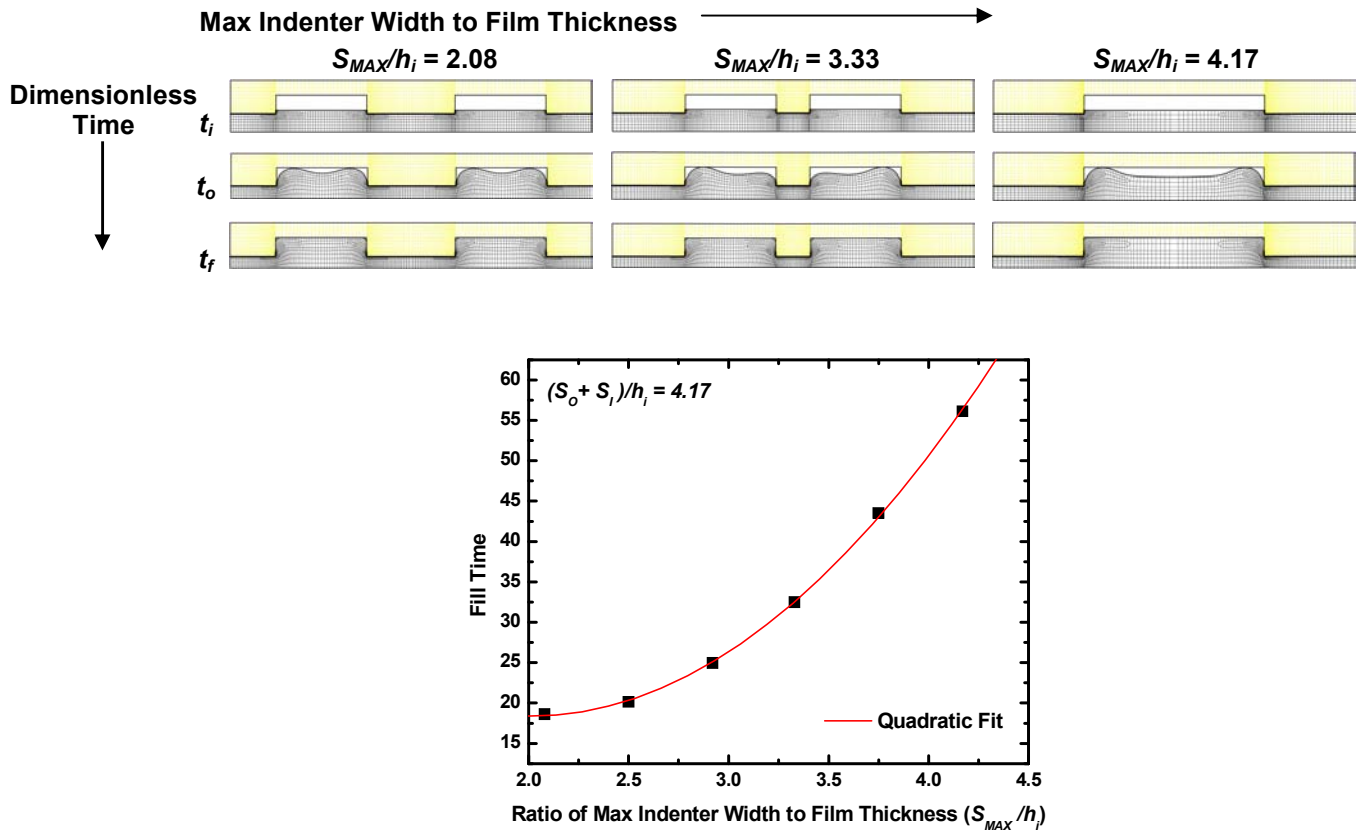
Figure 4. Fill times for various indenter width ratios with total indenter width constant. The quadratic fill time dependence on indenter width ratio shows that squeeze flow fill time is characterized by the maximum indenter width of the system.

The fill time dependence on the maximum indenter width has consequences for global replication time. In common embossing applications, S_{MAX}/h_i usually is or becomes > 1, thus governing relations based on squeeze flow apply [10]. The quadratic dependence of fill time based on maximum indenter width shown in Fig. 4 allows prediction of filling time. Figure 5 shows global fill time based on local cavity size. When large differences in cavity size exist, certain individual cavities quickly fill relative to the global filling time, and the embossing condition closely approximates squeeze flow of an indenter width that includes the filled cavity width. The close correlation of the single indenter, three cavity geometry, and squeeze limit geometry at large differences of outer and inner cavity sizes illustrates the validity of a global squeeze flow approximation. At larger negative differences of outer and inner cavity sizes than shown in Fig. 5, the fill time of the three cavity geometry will again approach the fill time of the limiting squeeze flow case.

For global mold design of a non-uniform embossing tool, maximum indenter width governs global filling time. In combined large scale and nano-scale imprinting, the quickly filled nano-scale cavities will represent a larger effective maximum indenter
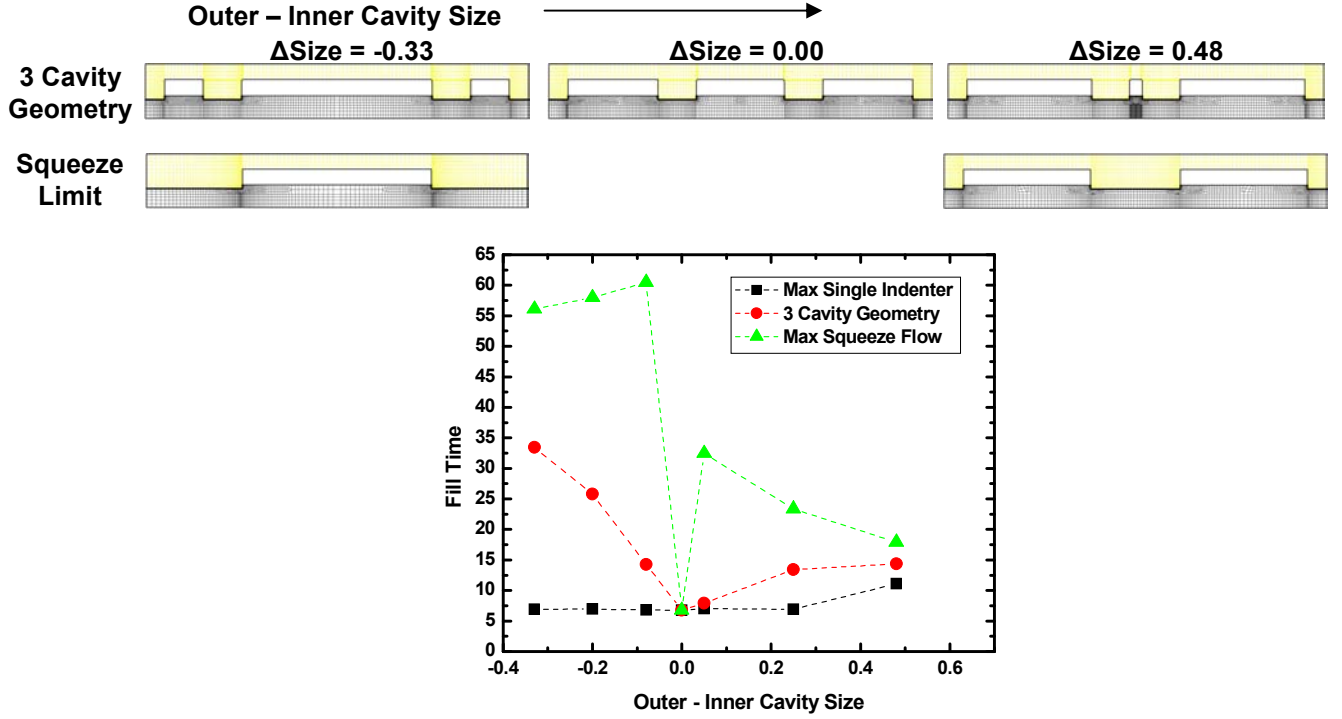
Figure 5. Cavity Size governs filling. Small cavity sizes generally fill first unless small cavities deform via a constrained single polymer peak. Large differences in cavity size increase fill time. Lower bound is maximum time to fill of a single, symmetric cavity. Upper bound is maximum time to fill for a squeeze flow configuration assuming one cavity initially filled. Global filling of molds can be approximated by squeeze flow of polymer over large areas.

width than the maximum indenter width prior to embossing. Areas of slow-filling constrained single peak flow can also be approximated for global mold design as a filled area representing a maximum indenter width, since ample polymer supply is available to locally fill the cavities and excess polymer must be transported to other regions of the mold. With knowledge of field dimensions, a global time to fill can be determined from a piecewise filling of smaller geometries with

$$t_{NIL} = \frac{\eta}{2P} \sum_{i=1}^{N} S_{MAX,i}{}^2 \left(\frac{1}{h_{r,i}{}^2} - \frac{1}{h_{r,i-1}{}^2} \right), \tag{2}$$

where $S_{MAX,i}$ and $h_{r,i}$ depend on the filling of areas of locally small cavities. When cavity sizes vary greatly over a global embossing tool, due to the quadratic dependence of fill time on indenter width, the limiting effective S_{MAX} can alone dominate the fill time. The filled small-sized flow field characterizing non-uniform embossing agrees well with

16

reports that long-range residual layer uniformity resulting from polymer flow between sections of different pattern density is independent of pattern size [13].

5. Conclusions

This paper reports simulations of viscous polymer flow during NIL replication of non-uniform embossing geometries. Individual cavity characteristic V_{NIL} determines cavity filling order. Relative cavity size and indenter width govern local polymer deformation. Large differences in cavity size lead to non-uniform filling and non-local polymer flow. Maximum indenter width governs filling time with a quadratic dependence and the rapid filling of small cavities results in an increase in effective maximum indenter width.

These simulations suggest that non-uniform embossing tool design should be tailored based on the principles of squeeze flow. Local filling of small cavities could be accommodated by designing embossing tools with symmetric filling over the total stamp area to reduce tool warping. Process design could be tailored by increasing temperature and introducing plasticizers to reduce polymer viscosity. By designing a single, non-uniform embossing tool with knowledge of irregular filling and squeeze flow, simultaneous full replication of large-scale and nano-scale patterns and near-uniform residual layer thickness can be achieved over a predicted time scale.

6. References

1. Chou, S. and P. Krauss, *Imprint lithography with sub-10 nm feature size and high throughput.* Microelectronic Engineering, 1997. **35**: p. 237-240.
2. Khang, D. and H. Lee, *Wafer-scale sub-micron lithography.* Applied Physics Letters, 1999. **75**: p. 2599-2601.
3. Cross, G.L.W., et al., *The Mechanics of Nanoimprint Forming.* Materials Research Society Symposium Proceedings, 2004. **841**.
4. Cross, G.L.W., B.S. O'Connell, and J.B. Pethica, *Influence of Elastic Strains on the Mask Ratio in Glassy Polymer Nanoimprint.* Applied Physics Letters, 2005. **86**(8): p. 081902.
5. Heyderman, L.J., et al., *Flow behaviour of thin polymer films used for hot embossing lithography.* Microelectronic Engineering, 2000. **54**: p. 229-245.
6. Hirai, Y., et al., *Study of the resist deformation in nanoimprint lithography.* Journal of Vacuum Science and Technology B, 2001. **19**(6): p. 2811-2815.
7. Hirai, Y., et al., *Simulation and experimental study of polymer deformation in nanoimprint lithography.* Journal of Vacuum Science and Technology B, 2004. **22**(6): p. 3288-3293.
8. Jeong, J.-H., et al., *Flow Behavior at the Embossing Stage of Nanoimprint Lithography.* Fibers and Polymers, 2002. **3**(3): p. 113-119.
9. Rowland, H.D. and W.P. King, *Polymer deformation and filling modes during microembossing.* Journal of Micromechanics and Microengineering, 2004. **14**: p. 1625-1632.
10. Rowland, H.D., et al., *Impact of polymer film thickness and cavity size on polymer flow during embossing: towards process design rules for nanoimprint lithography.* IEEE Transactions on Nanotechnology, 2005 (submitted).
11. Gourgon, C., et al., *Influence of pattern density in nanoimprint lithography.* Journal of Vacuum Science and Technology B, 2003. **21**(1): p. 98-105.
12. Scheer, H.C. and H. Schulz, *A contribution to the flow behaviour of thin polymer films during hot embossing lithography.* Microelectronic Engineering, 2001. **56**: p. 311-332.
13. Schulz, H., M. Wissen, and H.C. Scheer, *Local mass transport and its effect on global pattern replication during hot embossing.* Microelectronic Engineering, 2003. **67-68**: p. 657-663.
14. Young, W.-B., *Analysis of the nanoimprint lithography with a viscous model.* Microelectronic Engineering, 2005. **77**: p. 405-411.
15. Cheng, X. and L.J. Guo, *One-step lithography for various size patterns with a hybrid mask-mold.* Microelectronic Engineering, 2004. **71**: p. 288-293.
16. Colburn, M., et al. *Step and flash imprint lithography: a new approach to high-resolution patterning.* in *SPIE Emerging Lithographic Technologies III.* 1999: SPIE.
17. Xia, Q., et al., *Ultrafast patterning of nanostructures in polymers using laser assisted nanoimprint lithography.* Applied Physics Letters, 2003. **83**(21): p. 4417-4419.

18. Kim, H.Y., K.-s. Kim, and B.-h. Kim. *Micro/nano patterning characteristics in hot embossing process*. in *AIP Conference Proceedings*. 2004.

19. Sackinger, P.A., P.R. Schunk, and R.R. Rao, *A Newton-Raphson Pseudo-Solid Domain Mapping Technique for Free and Moving Boundary Problems: A Finite Element Implementation.* Journal of Computational Physics, 1996. **125**: p. 83-103.

20. Schunk, P.R., *TALE: An Arbitrary Lagrangian-Eulerain Approach to Fluid-Structure Interaction Problems*, in *Sandia Technical Report*. 1999 (unpublished), Sandia National Laboratories.

Distribution:

1	MS9409	Chris Moen	08757
1	MS0824	Wahid Hermina	01510
1	MS0834	Joel Lash	01514
1	MS9161	Bob Nilson	08764
1	MS0834	Pat Notz	01514
1	MS0834	Carlton Brooks	01512
1	MS0834	Chris Bourdon	01512
1	MS1245	John Emerson	02453
2	MS9018	Central Technical Files	8944
2	MS0899	Technical Library	9536
1	MS0188	D. Chavez, LDRD Office	1030
1	MS0115	CRADA Administration	1323
1	MS0161	Patent and Licensing Office	11500